

Strong renormalization of the Fermi-surface topology close to the Mott transition

Luca F. Tocchio,¹ Federico Becca,² and Claudius Gros¹

¹*Institute for Theoretical Physics, University of Frankfurt,
Max-von-Laue-Straße 1, D-60438 Frankfurt a.M., Germany*

²*CNR-IOM-Democritos National Simulation Centre and International School
for Advanced Studies (SISSA), Via Bonomea 265, I-34136, Trieste, Italy*

(Dated: November 5, 2018)

The underlying Fermi surface is a key concept for strongly-interacting electron models and has been introduced to generalize the usual notion of the Fermi surface to generic (superconducting or insulating) systems. By using improved correlated wave functions that contain backflow and Jastrow terms, we examine the two-dimensional $t-t'$ Hubbard model and find a non-trivial renormalization of the topology of the underlying Fermi surface close to the Mott insulator. Moreover, we observe a sharp crossover region, which arises from the metal-insulator transition, from a weakly interacting metal at small coupling to a resonating valence-bond superconductor at intermediate coupling. A violation of the Luttinger theorem is detected at low hole dopings.

PACS numbers: 71.27.+a, 71.18.+y, 71.30.+h, 74.20.-z, 74.72.-h

I. INTRODUCTION

The single-band Hubbard model with extended hopping on the square lattice has been widely investigated since the appearance of the high-temperature superconductors. Indeed, it is believed to represent the minimal model that is necessary to describe the electronic correlations in the Copper-Oxygen planes of Cuprate materials. A very rich variety of phases has been discussed in this context, including antiferromagnetism, superconductivity, charge-density waves, and non-Fermi-liquid metals.¹ Studies with various numerical techniques, ranging from dynamical mean-field theory (DMFT),² including its cluster extensions,³⁻⁷ to quantum Monte Carlo techniques,⁸⁻¹² as well as analytic approaches,^{13,14} have addressed hotly debated topics like the nature of the pseudo-gap phase or the superconducting correlations.

Landau¹⁵ and Luttinger¹⁶ have shown that the Fermi surface, which is the locus of gapless electronic excitations in k -space, represents a pivoting concept in the theory of Fermi liquids. The generalization of this notion for gapped systems (e.g., superconductors or Mott insulators) leads to the idea that there is an underlying Fermi surface that becomes gapped because of some symmetry breaking (leading to superconductivity) or electronic correlation (leading to a Mott insulator). In particular, the underlying Fermi surface can be defined by the locus of points where $\text{Re}G(k, \omega = 0)$ changes sign ($G(k, \omega)$ is the single-particle Green's function), passing either to infinity (for usual Fermi liquids with well defined quasiparticles) or to zero.¹⁷ The question of determining the underlying Fermi surface is of central importance in strongly correlated systems, particularly in view of experiments with angle-resolved photoemission spectroscopy (ARPES).¹⁸ From the theoretical point of view, there are few attempts to study the topology of the Fermi surface in correlated systems; furthermore, they are limited to mean-field approaches,¹⁹⁻²¹ including recent calculations with cluster DMFT.²² Here, we make

a substantial step forward and consider non-perturbative calculations directly in a two-dimensional system. We use variational wave functions containing backflow correlations, which have been shown to be very accurate in the Hubbard model,^{23,24} and focus our attention on the topology of the underlying Fermi surface and the superconducting properties. We show that a strong renormalization of the underlying Fermi surface takes place close to half filling, when the Mott insulator is approached. In particular, the renormalization to perfect nesting occurring at the interaction-driven metal-insulator transition opens a new perspective on the crucial role of momentum dependence in describing the Mott transition.

At finite dopings we find a sharp crossover line, which emerges from the Mott-Hubbard transition point at half filling and separates a weakly-correlated metal and a strong-coupling superconducting state, in agreement with a recent observation of an unconventional metallic state at finite dopings.²⁵ Our findings could be also related to a recently proposed first-order line separating two metallic phases, one with a pseudogap and one without.²⁶ For the superconducting order parameter we obtain a sizable signal for moderately large on-site interactions, i.e., $U/t \simeq 7 - 10$.

The paper is organized as follows: in section II, we introduce the Hamiltonian and describe our variational wave function; in section III, we present our numerical results and, finally, in section IV we draw the conclusions.

II. MODEL AND VARIATIONAL WAVE FUNCTION

We consider the Hubbard model with extended hopping on a two-dimensional square lattice,

$$\mathcal{H} = -t \sum_{\langle ij \rangle \sigma} c_{i\sigma}^\dagger c_{j\sigma} - t' \sum_{\langle\langle ij \rangle\rangle \sigma} c_{i\sigma}^\dagger c_{j\sigma} + \text{h.c.} + U \sum_i n_{i\uparrow} n_{i\downarrow}, \quad (1)$$

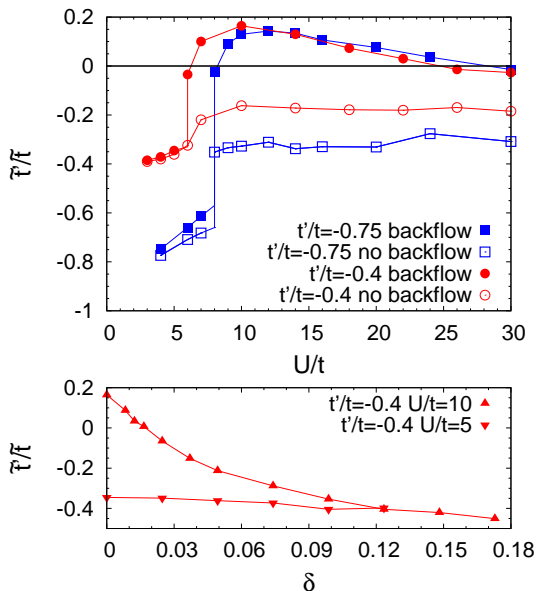


FIG. 1: (Color online) Upper panel: variational hopping ratio \tilde{t}'/\tilde{t} as a function of U/t for $t'/t = -0.4$ and -0.75 . Full (empty) symbols refer to the presence (absence) of backflow correlations in the variational wave function. Lower panel: variational hopping ratio \tilde{t}'/\tilde{t} as a function of the doping δ for $U/t = 5$ and 10 with $t'/t = -0.4$. Here, only results with backflow terms are shown. Data are shown for a $L = 162$ lattice; in the lower panel few points on a $L = 242$ lattice are added close to half filling.

where $c_{i\sigma}^\dagger$ ($c_{i\sigma}$) denotes the electron creation (destruction) operator of one electron on site i with spin $\sigma = \uparrow, \downarrow$, $\langle ij \rangle$ and $\langle\langle ij \rangle\rangle$ indicate nearest and next-nearest neighbor sites respectively; $n_{i\sigma} = c_{i\sigma}^\dagger c_{i\sigma}$ is the electron density; t and t' are the nearest and next-nearest neighbor hopping amplitudes, and U is the on-site Coulomb repulsion. Calculations are performed on 45-degree tilted clusters with $L = 2 \times l^2$ sites (l being an odd integer) and periodic boundary conditions. The number of electrons is N , such that the hole doping is $\delta = 1 - n$, with $n = N/L$.

The question of determining the underlying Fermi surface has been addressed by using a renormalized mean-field approach in Refs. 19,20. Here, we include electronic correlations in a non-perturbative way. In a first step, we construct uncorrelated wave functions given by the ground state $|\text{BCS}\rangle$ of a superconducting Bardeen-Cooper-Schrieffer (BCS) Hamiltonian:^{27,28}

$$\mathcal{H}_{\text{BCS}} = \sum_{k\sigma} \xi_k c_{k\sigma}^\dagger c_{k\sigma} + \sum_k \Delta_k c_{k\uparrow}^\dagger c_{-k\downarrow}^\dagger + \text{h.c.}, \quad (2)$$

where both the free-band dispersion ξ_k and the pairing amplitudes Δ_k are variational functions. We use the parametrization

$$\xi_k = -2\tilde{t}(\cos k_x + \cos k_y) - 4\tilde{t}' \cos k_x \cos k_y - \mu \quad (3)$$

$$\Delta_k = 2\Delta_{\text{BCS}}(\cos k_x - \cos k_y), \quad (4)$$

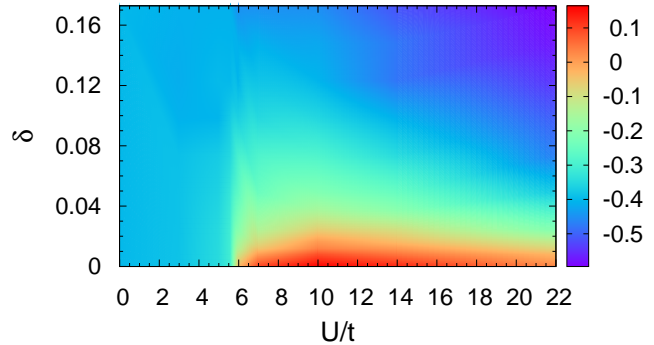


FIG. 2: (Color online) Variational hopping ratio \tilde{t}'/\tilde{t} as a function of doping δ and U/t for the case with $t'/t = -0.4$. The density plot is obtained by using results with $L = 162$ and 242 .

where the effective hopping amplitude \tilde{t}' , the effective chemical potential μ , and the local pairing field Δ_{BCS} are variational parameters to be optimized. The parameter \tilde{t} is kept fixed to set the energy scale. We also considered longer-range effective hopping parameters in Eq. (4) finding that all hoppings beyond the ones present in the Hamiltonian (1) are optimized to zero.

The correlated state $|\Psi_{\text{BCS}}\rangle$, without backflow terms, is then given by $|\Psi_{\text{BCS}}\rangle = \mathcal{J}|\text{BCS}\rangle$, where $\mathcal{J} = \exp(-1/2 \sum_{ij} v_{ij} n_i n_j)$ is a density-density Jastrow factor (including the on-site Gutzwiller term v_{ii}), with the v_{ij} 's being optimized for every independent distance $|i - j|$. Notably, within this kind of wave function, it is possible to obtain a pure (i.e., non-magnetic) Mott insulator for a sufficiently singular Jastrow factor $v_q \sim 1/q^2$ (v_q being the Fourier transform of v_{ij}), while a superconducting (metallic) state is found whenever $v_q \sim 1/q$ and $\Delta_{\text{BCS}} > 0$ ($\Delta_{\text{BCS}} = 0$).²⁹

A size-consistent and efficient way to further improve the correlated state $|\Psi_{\text{BCS}}\rangle$ for large on-site interactions is based on backflow correlations. In this approach, each orbital that defines the unprojected state $|\text{BCS}\rangle$ is taken to depend upon the many-body configuration, such to incorporate virtual hopping processes.^{23,24} All results presented here are obtained by fully incorporating the backflow corrections and optimizing individually every variational parameter in ξ_k and Δ_k , in the Jastrow factor \mathcal{J} , as well as for the backflow corrections.

III. RESULTS

A. Fermi-surface renormalization

We start our analysis by discussing the evolution of the underlying Fermi surface topology as a function of hole doping δ and interaction strength U/t . Within the varia-

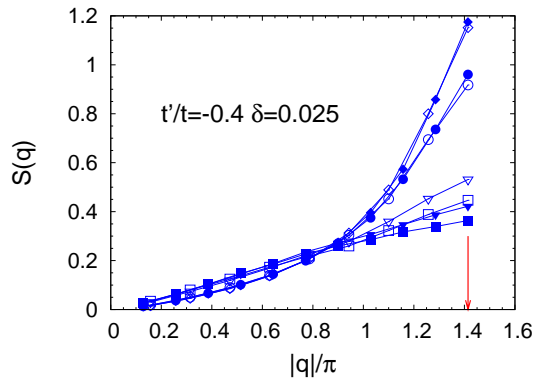


FIG. 3: (Color online) Static spin-spin correlations $S(q)$ as a function of $|q|/\pi$ along the $\Gamma = (0, 0)$ to $M = (\pi, \pi)$ direction, for $t'/t = -0.4$. Data are presented for $U/t = 5$ (squares), $U/t = 5.6$ (triangles), $U/t = 6$ (circles) and $U/t = 7$ (diamonds). Full (empty) symbols refer to $L = 242$ ($L = 162$). The location of the point $Q = (\pi, \pi)$ is marked with an arrow.

tional approach, the underlying Fermi surface can be easily defined and corresponds to the highest occupied momenta ξ_k . Indeed, $E_k = \sqrt{\xi_k^2 + \Delta_k^2}$ corresponds, within renormalized mean-field theory,²⁸ to the excitation spectrum of projected Bogoliubov modes and hence ξ_k to the dispersion of the renormalized quasiparticles. Here, we would like to stress that, although ξ_k corresponds to the “non-interacting” spectrum, it may be strongly renormalized because of the full optimization of the variational wave function: due to the presence of Jastrow and backflow terms, non-trivial values of \tilde{t}' and Δ_{BCS} may be obtained.

Firstly, we consider the half-filled case, where, by increasing the ratio U/t a metal-insulator transition is encountered. We present the results for $t'/t = -0.4$ and $t'/t = -0.75$, see Fig. 1. In both cases, a renormalization towards perfect nesting, namely $\tilde{t}'/\tilde{t} = 0$, is shown to occur both at the metal-insulator transition and in the limit $U/t \rightarrow \infty$. In the metallic phase, the ratio \tilde{t}'/\tilde{t} is only slightly modified with respect to its bare value, and this result is found both with and without backflow correlations, demonstrating that even the simple wave function without backflow may capture a correct description of the metallic phase. Then, at the metal-insulator transition, the variational ratio of the hopping parameters is strongly renormalized in presence of backflow correlations, i.e., $\tilde{t}'/\tilde{t} \rightarrow 0$, driving the underlying Fermi surface to be perfectly nested. This fact suggests that a full momentum resolution is a crucial ingredient to properly describe a metal-insulator transition. Remarkably, this renormalization does not occur if backflow correlations are not included. By further increasing the on-site Coulomb repulsion, the renormalized hopping ratio changes sign and then decreases again to zero at large U/t .³⁰ This renormalization, which is again possible only in presence of backflow correlations, is in agreement with renormalized mean-field studies of the t - J

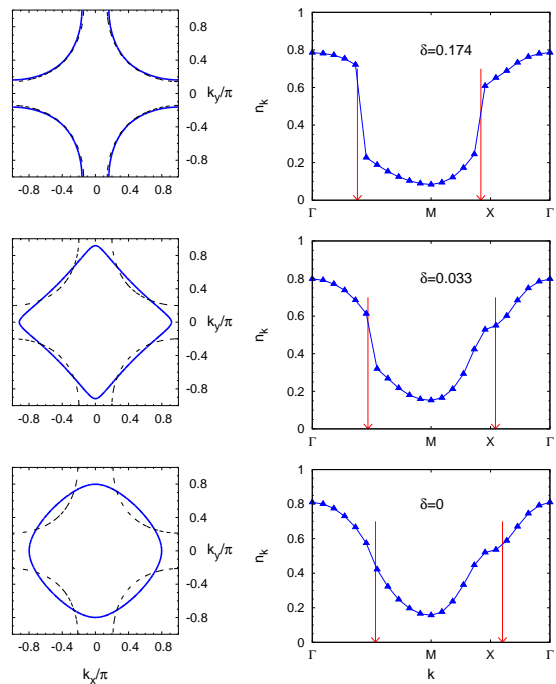


FIG. 4: (Color online) Left panels: the underlying Fermi surface defined by $\xi_k = 0$ (solid blue lines) and the non-interacting Fermi surface $\xi_k^0 = 0$ (dashed black lines) for the same parameter values of the corresponding right panels (see text for more details). Right panels: momentum distribution function n_k along the path in the Brillouin zone connecting the points $\Gamma = (0, 0)$, $M = (\pi, \pi)$, and $X = (\pi, 0)$. Data are shown at $U/t = 10$ and $t'/t = -0.4$ for a $L = 242$ lattice size at three dopings ($\delta = 0, 0.033$, and 0.174). Arrows indicate the position of the underlying Fermi surface, as found in left panels.

model,²⁰ where the Fermi surface renormalizes to perfect nesting for $\delta \rightarrow 0$, and with a slave-spin study of the Hubbard model in the large-interaction limit.²¹ Note that for $U/t > 25$ the numerical accuracy for the ratio \tilde{t}'/\tilde{t} is not enough to distinguish a finite from a vanishing value, see Fig. 1.

We would like to mention that a Fermi-surface renormalization close to the Mott transition has already been described in the one-dimensional Hubbard model.³¹ Also in that case, a perfectly nested Fermi surface, i.e., $k_F = \pm\pi/2$, is found. This consideration enforces the idea that the variational hopping ratio in two dimensions does not vanish accidentally at the Mott transition, but is renormalized in order to get perfect nesting of the underlying Fermi surface.

The variational hopping changes very rapidly by doping the Mott insulator and tends towards the bare value at high values of hole dopings, see the case $U/t = 10$ in Fig. 1. In summary, we present in Fig. 2 a complete density plot for the variational hopping \tilde{t}'/\tilde{t} as a function of doping δ and U/t , with bare $t'/t = -0.4$. While we have almost no renormalization when the half-filled case is metallic (i.e., for $U/t \lesssim 6$), we observe that a

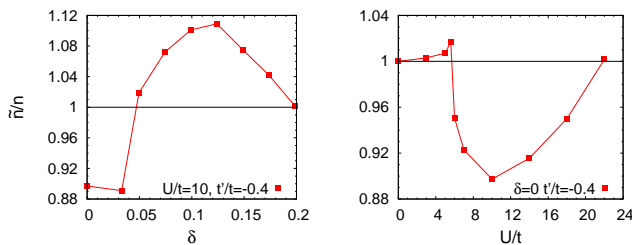


FIG. 5: (Color online) Left panel: Ratio between the number of electrons enclosed by the renormalized Fermi surface, \tilde{n} , and the number of electrons effectively present in the system, n , as a function of doping. Data refer to the case $U/t = 10$ and $L = 242$. Right panel: Same quantity as in the left panel as a function of U/t at half filling, for $L = 242$.

strong renormalization close to half filling is present for $U/t \gtrsim 6$. Remarkably, the metal-insulator transition occurring at half filling comes with a sharp crossover line at finite doping that we can characterize through an abrupt change in the value of \tilde{t}'/\tilde{t} . This crossover separates a weakly-correlated metal at low U/t and a strongly renormalized state at intermediate/strong values of U/t . This result is in agreement with a recent ARPES study on $\text{YBa}_2\text{Cu}_3\text{O}_{6+x}$, which found indications for an unconventional metallic state.²⁵

B. Magnetic correlations

We provide here further evidence of the sharp crossover line by calculating the static spin-spin correlations, defined as

$$S(q) = \frac{1}{L} \sum_{m,n} e^{iq(R_m - R_n)} \langle S_m^z S_n^z \rangle, \quad (5)$$

where S_m^z is the z -component of the spin operator on site m . The presence of (short-range) antiferromagnetic correlations is signaled by the appearance of a (non-diverging) peak in $S(q)$, located at $Q = (\pi, \pi)$. As shown in Fig. 3 for the doping $\delta = 0.025$, the correlated resonating-valence bond (RVB) state at $U/t \gtrsim 6$ is characterized by antiferromagnetic correlations that are strongly enhanced with respect to the metallic phase at $U/t \lesssim 6$. The two regimes are clearly separated by a jump in the value of $S(Q)$; the short-range nature of the antiferromagnetic correlations is confirmed by a size scaling study.

C. Momentum distribution function

In Fig. 4, we compare the results of the underlying Fermi surface with the ones for the momentum distribution $n_k = \langle c_{k\sigma}^\dagger c_{k\sigma} \rangle$, for $U/t = 10$ and three different dopings. Interestingly, in the low-doping regime, the area enclosed by $\xi_k = 0$ is different from the one

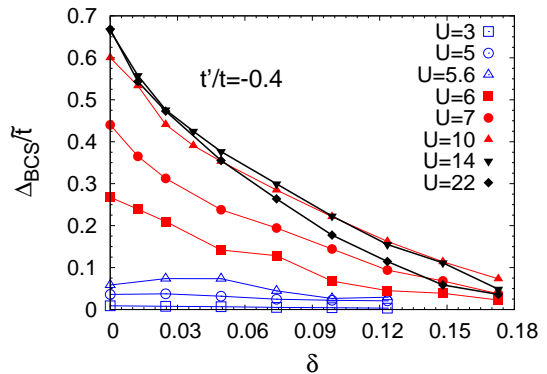


FIG. 6: (Color online) Pairing amplitude $\Delta_{\text{BCS}}/\tilde{t}$ as a function of doping for $t'/t = -0.4$ and different values of U/t . Data are presented for a $L = 162$ lattice size.

enclosed by the non-interacting system $\xi_k^0 = 0$, where $\xi_k^0 = -2t(\cos k_x + \cos k_y) - 4t' \cos k_x \cos k_y - \mu_0$, μ_0 being the bare chemical potential. At half filling, the underlying Fermi surface is closed, but the system is insulating and consistently n_k shows a completely smooth behavior. This is due to the presence of a strong Jastrow factor $v_q \sim 1/q^2$ which is able to remove the singularities present in $|\text{BCS}\rangle$.³² As soon as a small doping is considered, the system becomes conducting and a finite jump in n_k appears along the nodal direction $\Gamma \rightarrow M$, where the pairing amplitude Δ_k vanishes. At small dopings, the variational hopping \tilde{t}'/\tilde{t} undergoes an abrupt change (see Fig. 2) and, therefore, the Fermi surface becomes rapidly open, see Fig. 4. Finally, at large dopings, the superconducting gap vanishes and a full Fermi surface is recovered also in the momentum distribution, i.e., a finite jump is also detected along the $M \rightarrow X$ direction. Additional results on the evolution of the underlying Fermi surface as a function of doping for $U/t = 10$ and $U/t = 5$ can be found in the Appendix A.

In the large doping case, the jump along the $M \rightarrow X$ direction coincides with the position of the underlying Fermi surface. When the doping is small and there is no jump along the $M \rightarrow X$ direction, one could extend the previous concept and associate the location of the maximal gradient of n_k with the position of the underlying Fermi surface. However, as shown in Fig. 4, this approach would lead to incorrect results, since the underlying Fermi surface is closer to the X point with respect to the location of the maximal gradient. Therefore, our results suggest that, when doping is small and electronic correlation is important, some caution should be taken in deriving the Luttinger surface from the location of the maximal gradient of n_k ,^{33,34} similarly to what has been discussed in Ref. 20 for the t - J model.

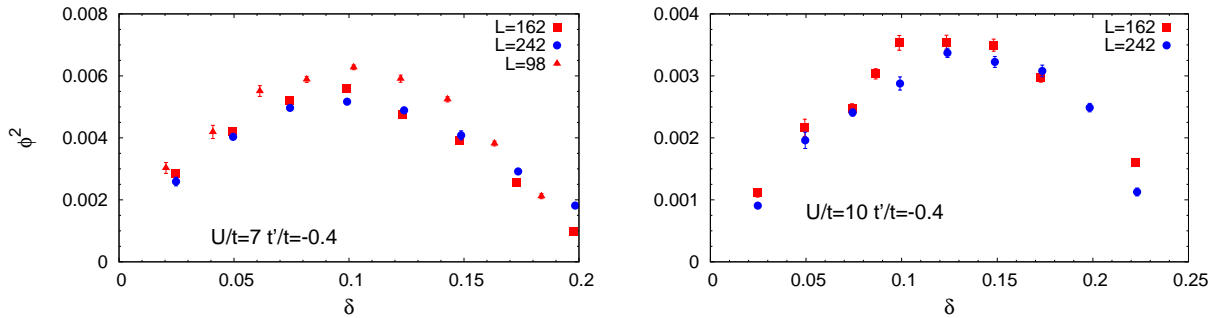


FIG. 7: (Color online) Superconducting order parameter squared ϕ^2 as a function of doping for $t'/t = -0.4$ and $U/t = 7$ (left panel) and $U/t = 10$ (right panel).

D. Luttinger sum rule

The renormalization of the underlying Fermi surface leads to a violation of the Luttinger sum rule. Let us denote by \tilde{n} the number of electrons that are enclosed by the renormalized Fermi surface $\xi_k = 0$. As shown in Fig. 4, close to half filling, the $\xi_k = 0$ contour is electron-like, containing less electrons than n , i.e., $\tilde{n}/n < 1$, while for $0.05 \lesssim \delta \lesssim 0.2$, the contour is hole-like and $\tilde{n}/n > 1$. For larger values of the doping, the Luttinger count holds. The summary for the Luttinger sum rule is reported in Fig. 5. Our results are slightly different from the ones found at the simple mean-field level,¹⁹ especially close to the Mott insulator where we find that $\delta n \simeq -0.1$. In Fig. 5, we also present the violation of the Luttinger sum rule at half filling, as a function of U/t . In the insulating state ($U/t \gtrsim 6$) the underlying Fermi surface defined by $\xi_k = 0$ encloses less electrons than n . This result is compatible with the electron-like nature of the contour, due to the strong renormalization of the variational hopping parameters. On the contrary, in the metallic region we only observe a tiny violation, in particular close to the metal-insulator transition. This tiny violation can be related to the amount of correlation present in the low- U metallic state and it is indeed significantly smaller than the degree of correlation that can be observed in the RVB state emerging from the Mott insulator upon doping, see Fig 5.

E. Pairing amplitude and pair-pair correlations

We discuss now the variational pairing amplitude Δ_{BCS} , which measures the tendency to create resonating singlets, and the actual pair-pair correlations $\langle \Delta(r) \rangle = \langle S_r S_0^\dagger \rangle$, where $S_r^\dagger = c_{r\uparrow}^\dagger c_{r+x\downarrow}^\dagger - c_{r\downarrow}^\dagger c_{r+x\uparrow}^\dagger$. At weak-coupling (when a conducting state is found at half filling), Δ_{BCS} remains relatively small and does not change much with doping, see Fig 6. For $U/t \gtrsim 6$ (when an insulating state is found at half filling), Δ_{BCS} has a sizable value and decreases monotonically as a function of the doping. This behavior of the pairing amplitude has been

related to the pseudo-gap of the normal phase of Cuprate materials.¹⁰

In Fig 7, we report the results for the superconducting order parameter $\phi^2 = \lim_{r \rightarrow \infty} \Delta(r)$, similarly to what has been done in previous calculations for the Hubbard and $t - J$ models.^{10,35} Our results are presented for $U/t = 7$ and 10 , where superconductivity develops at finite doping. For smaller values of the on-site interactions, a much smaller signal is obtained. By increasing U/t , the optimal doping becomes larger and the magnitude of the order parameter decreases, suggesting that intermediate values of U/t are optimal for maximal critical temperatures T_c , when assuming that T_c scales with ϕ .

IV. CONCLUSIONS

Our calculations represent a first attempt to trace the Fermi surface renormalization in a truly two-dimensional system where the electron-electron correlation is treated beyond simple mean-field approaches. A substantial deviation from the Luttinger sum rule is observed for large values of U/t , where the topology of the underlying Fermi surface changes from electron-like to hole-like by increasing the doping. It would be very interesting to verify these results on correlated materials, like Cuprate superconductors, where ARPES probes should be able to detect changes in the topology of the Fermi surface.

Furthermore, we show evidence of a sharp crossover region that originates from the metal-insulator transition and separates a weakly-correlated metal from a more correlated RVB superconductor at low dopings.

L.F.T. and C.G. acknowledge the support of the German Science Foundation through the Transregio 49.

Appendix A: Underlying Fermi surface

In Fig. 8, we present a systematic plot of the underlying Fermi surface defined by the contour $\xi_k = 0$ and of the non-interacting Fermi surface, $\xi_k^0 = 0$, as a function of

doping for the case $U/t = 10$. The underlying Fermi surface evolves from electron-like, when $\delta \lesssim 0.05$, to hole-like, for $\delta \gtrsim 0.05$. When $\delta \sim 0.2$ the underlying Fermi surface becomes very close to the non-interacting one, as expected when doping becomes large and electronic correlation consequently less important.

In Fig. 9, we present also a plot of the underlying Fermi

surface as a function of doping for $U/t = 5$. In this regime, the half-filled case is metallic and the renormalization of the variational parameters is very weak. Consequently, the underlying Fermi surface does not show a remarkable evolution as a function of doping and almost coincides with the non-interacting contour.

-
- ¹ See for example, E.W. Carlson, V.J. Emery, S.A. Kivelson, D. Orgad, *Concepts in high-temperature superconductivity* in “The Physics of Conventional and Unconventional Superconductors” ed. by K.H. Bennemann and J.B. Ketterson (Springer-Verlag, 2003).
- ² A. Georges, G. Kotliar, W. Krauth, and M.J. Rozenberg, *Rev. Mod. Phys.* **68**, 13 (1996).
- ³ T.A. Maier, M. Jarrell, T.C. Schulthess, P.R.C. Kent, and J.B. White, *Phys. Rev. Lett.* **95**, 237001 (2005).
- ⁴ S.S. Kancharla, B. Kyung, D. Senechal, M. Civelli, M. Capone, G. Kotliar, and A.-M.S. Tremblay, *Phys. Rev. B* **77**, 184516 (2008).
- ⁵ M. Civelli, *Phys. Rev. B* **79**, 195113 (2009).
- ⁶ K.-S. Chen, S. Pathak, S.-X. Yang, S.-Q. Su, D. Galanakis, K. Mielson, M. Jarrell, and J. Moreno, *Phys. Rev. B* **84**, 245107 (2011).
- ⁷ S.-X. Yang, H. Fotsos, S.-Q. Su, D. Galanakis, E. Khatami, J.-H. She, J. Moreno, J. Zaanen, and M. Jarrell, *Phys. Rev. Lett.* **106**, 047004 (2011).
- ⁸ J.E. Hirsch, *Phys. Rev. B* **31**, 4403 (1985).
- ⁹ S.R. White, D.J. Scalapino, R.L. Sugar, E.Y. Loh, J.E. Gubernatis, and R.T. Scalettar, *Phys. Rev. B* **40**, 506 (1989).
- ¹⁰ A. Paramekanti, M. Randeria, and N. Trivedi, *Phys. Rev. Lett.* **87**, 217002 (2001).
- ¹¹ S. Sorella, G.B. Martins, F. Becca, C. Gazza, L. Capriotti, A. Parola, and E. Dagotto, *Phys. Rev. Lett.* **88**, 117002 (2002).
- ¹² C.N. Varney, C.-R. Lee, Z.J. Bai, S. Chiesa, M. Jarrell, and R.T. Scalettar, *Phys. Rev. B* **80**, 075116 (2009).
- ¹³ K.-Y. Yang, T.M. Rice, and F.-C. Zhang, *Phys. Rev. B* **73**, 174501 (2006).
- ¹⁴ B.S. Shastry, *Phys. Rev. Lett.* **107**, 056403 (2011); see also G.H. Gweon, B.S. Shastry, and G.D. Gu, *Phys. Rev. Lett.* **107** 056404 (2011).
- ¹⁵ L.D. Landau, *JETP* **3**, 920 (1957).
- ¹⁶ J.M. Luttinger, *Phys. Rev.* **119**, 1153 (1960).
- ¹⁷ I. Dzyaloshinskii, *Phys. Rev. B* **68**, 085113 (2003).
- ¹⁸ H.B. Yang, J.D. Rameau, Z.-H. Pan, G.D. Gu, P.D. Johnson, H. Claus, D.G. Hinks, and T.E. Kidd, *Phys. Rev. Lett.* **107**, 047003 (2011).
- ¹⁹ R. Sensarma, M. Randeria, and N. Trivedi, *Phys. Rev. Lett.* **98**, 027004 (2007).
- ²⁰ C. Gros, B. Edegger, V.N. Muthukumar, and P.W. Anderson, *PNAS* **103**, 14298 (2006).
- ²¹ A. Rüegg, S.D. Huber, M. Sigrist, *Phys. Rev. B* **81**, 155118 (2010).
- ²² M. Civelli, M. Capone, S.S. Kancharla, O. Parcollet, and G. Kotliar, *Phys. Rev. Lett.* **95**, 106402 (2005).
- ²³ L.F. Tocchio, F. Becca, A. Parola, and S. Sorella, *Phys. Rev. B* **78**, 041101(R) (2008); see also, F. Becca, L.F. Tocchio, and S. Sorella, *J. Phys.: Conf. Ser.* **145**, 012016 (2009).
- ²⁴ L.F. Tocchio, F. Becca, and C. Gros, *Phys. Rev. B* **83**, 195138 (2011).
- ²⁵ D. Fournier, G. Levy, Y. Pennec, J.L. McChesney, A. Bostwick, E. Rotenberg, R. Liang, W. N. Hardy, D.A. Bonn, I. S. Elfimov, and A. Damascelli, *Nature Physics* **6**, 905 (2010).
- ²⁶ G. Sordi, P. Sémon, K. Haule, and A.-M. S. Tremblay, *arXiv:1110.1392* (2011).
- ²⁷ C. Gros, *Phys. Rev. B* **38**, 931(R) (1988).
- ²⁸ F.C. Zhang, C. Gros, T.M. Rice, and H. Shiba, *Supercond. Sci. Technol.* **1**, 36 (1988).
- ²⁹ M. Capello, F. Becca, M. Fabrizio, S. Sorella, and E. Tosatti, *Phys. Rev. Lett.* **94**, 026406 (2005).
- ³⁰ At half filling, the sign of t' (and, consistently \tilde{t}') is irrelevant. We take the same sign (negative) that is used at finite dopings.
- ³¹ L.F. Tocchio, F. Becca, and C. Gros, *Phys. Rev. B* **81**, 205109 (2010).
- ³² M. Capello, F. Becca, S. Yunoki, and S. Sorella, *Phys. Rev. B* **73**, 245116 (2006).
- ³³ M. Randeria, H. Ding, J.-C. Campuzano, A. Bellman, G. Jennings, T. Yokoya, T. Takahashi, H. Katayama-Yoshida, T. Mochiku, and K. Kadowaki, *Phys. Rev. Lett.* **74**, 4951 (1995).
- ³⁴ J. Mesot, M. Randeria, M.R. Norman, A. Kaminski, H.M. Fretwell, J.C. Campuzano, H. Ding, T. Takeuchi, T. Sato, T. Yokoya, T. Takahashi, I. Chong, T. Terashima, M. Takano, T. Mochiku, and K. Kadowaki, *Phys. Rev. B* **63**, 224516 (2001).
- ³⁵ L. Spanu, M. Lugas, F. Becca, and S. Sorella, *Phys. Rev. B* **77**, 024510 (2008).

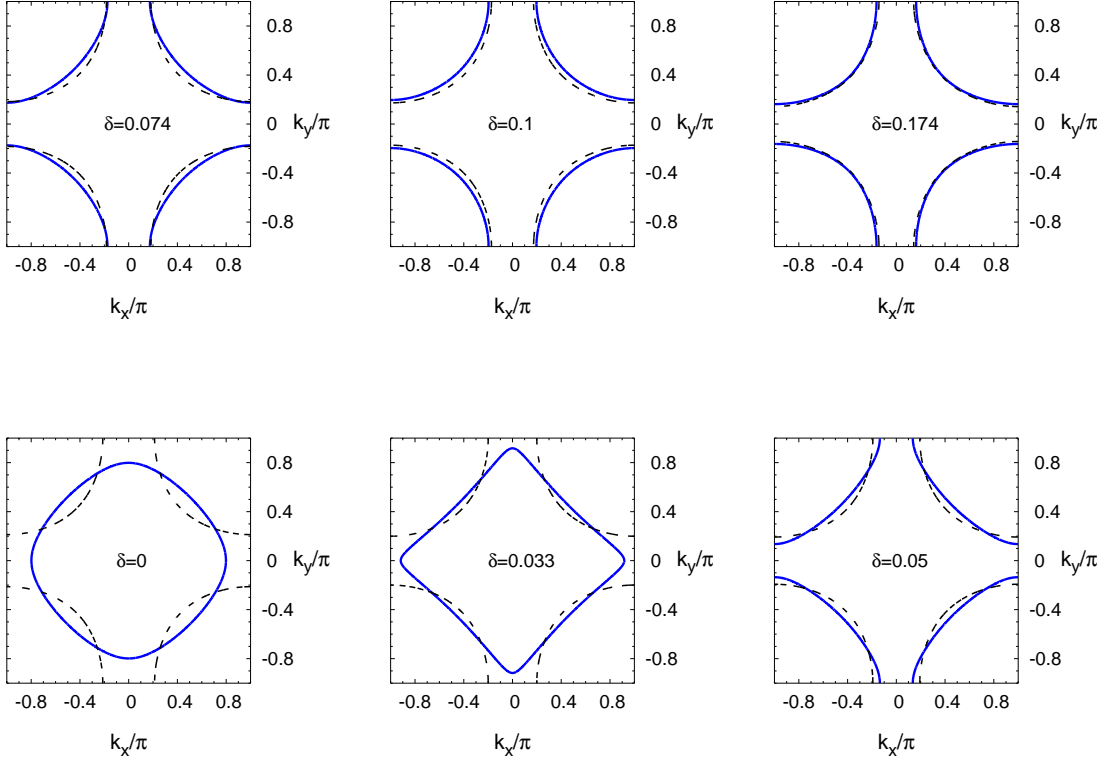


FIG. 8: (Color online) The underlying Fermi surface defined by $\xi_k = 0$ (solid blue lines) and the non-interacting Fermi surface $\xi_k^0 = 0$ (dashed black lines) as a function of doping. Data are presented at $U/t = 10$ for $L = 242$.

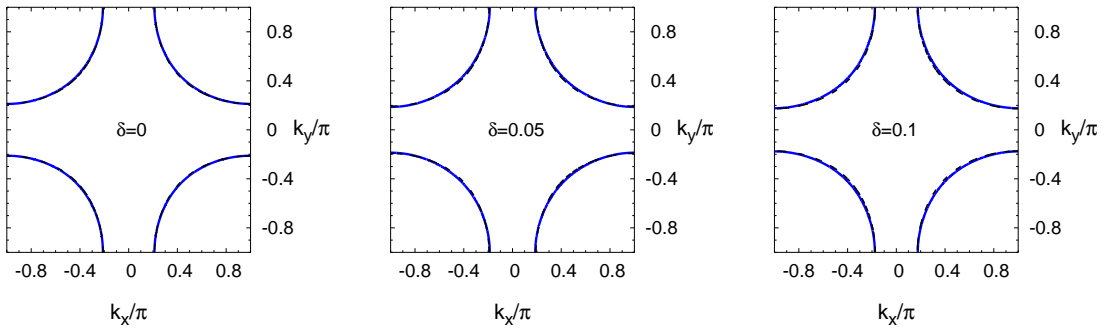


FIG. 9: (Color online) The underlying Fermi surface defined by $\xi_k = 0$ (solid blue lines) and the non-interacting Fermi surface $\xi_k^0 = 0$ (dashed black lines) as a function of doping. Data are presented at $U/t = 5$ for $L = 242$.